THE ASTROPHYSICAL JOURNAL, 465:L15–L18, 1996 July 1

OPTICAL ROTATION CURVES OF DISTANT FIELD GALAXIES: KECK RESULTS AT REDSHIFTS TO $z \sim 1$[1, 2]

NICOLE P. VOGT, DUNCAN A. FORBES, ANDREW C. PHILLIPS, CARYL GRONWALL,
S. M. FABER, GARTH D. ILLINGWORTH, AND DAVID C. KOO
University of California Observatories/Lick Observatory, Board of Studies in Astronomy and Astrophysics, University of California, Santa Cruz, CA 95064
Received 1996 March 27; accepted 1996 April 19

ABSTRACT

Spatially resolved velocity profiles are presented for nine faint field galaxies in the redshift range $0.1 \lesssim z \lesssim 1$, based on moderate-resolution spectroscopy obtained with the Keck 10 m telescope. These data were augmented with high-resolution *Hubble Space Telescope* images from WFPC2, which provided V and I photometry, galaxy type, orientation, and inclination. The effects of seeing, slit width, and slit misalignment with respect to galaxy major axis were modeled along with inclination for each source, in order to derive a maximum circular velocity from the observed rotation curve. The lowest redshift galaxy, though highly elongated, shows a distorted low-amplitude rotation curve that suggests a merger in progress seen perpendicular to the collision path. The remaining rotation curves appear similar to those of local galaxies in both form and amplitude, implying that some massive disks were in place at $z \sim 1$. The key result is that the kinematics of these distant galaxies show evidence for only a *modest* increase in luminosity ($\Delta M_B \lesssim 0.6$) compared to velocity-luminosity (Tully-Fisher) relations for local galaxies.

Subject headings: galaxies: evolution — galaxies: kinematics and dynamics

1. INTRODUCTION

The rotational velocity and luminosity of disk galaxies are found to be strongly correlated (Roberts, Roberts, & Shu 1975; Tully & Fisher 1977). This scaling relation—the "Tully-Fisher (TF) relation"—provides a powerful tool to tackle such problems as deriving H_0 (e.g., Pierce & Tully 1988), or mapping the local galaxy streaming motions (e.g., Aaronson et al. 1986). These studies have been confined to nearby galaxies by the use of single-dish H I radio observations (e.g., Haynes & Giovanelli 1991) or optical emission line spectra (e.g., Rubin et al. 1985; Mathewson, Ford, & Buchhorn 1992). Extending velocity width studies to more distant galaxies would be particularly valuable to investigate galaxy evolution (Kron 1986; van der Kruit & Pickles 1988). Current galaxy evolution models range from those with mild amounts of luminosity brightening in the past (e.g., Gronwall & Koo 1995) to those requiring more dramatic changes (e.g., Broadhurst, Ellis, & Shanks 1988; Colless et al. 1990; Glazebrook et al. 1995) to explain the large numbers of faint blue galaxies. By comparing a distant sample of rotation curves to local TF relations, we can directly constrain the global brightening of disk galaxies in the past.

The H I Tully-Fisher method is limited by the sensitivity of current radio telescopes to $z \lesssim 0.1$. Beyond this, two approaches have been used. Vogt et al. (1993) derived rotation curves from strong optical emission lines for two spirals at $z \sim 0.2$. Without spatial resolution, an alternative measure of distant spiral kinematics may be extracted from the velocity widths of emission lines. Forbes et al. (1996) measured velocity widths for a sample of 18 faint field galaxies with redshifts $0.2 < z < 0.84$, while Colless et al. (1994) examined the equivalent widths of [O II] for a sample of 26 field galaxies with redshifts $0.1 \lesssim z \lesssim 0.7$.

This paper presents rotation curves for nine field galaxies at redshifts $0.1 \lesssim z \lesssim 1$. This project combines spatially resolved spectra from the 10 m Keck telescope with inclinations and position angles determined from the refurbished *Hubble Space Telescope* (*HST*). These data provide a first glimpse into the internal kinematics of galaxies out to a redshift of $z \sim 1$, or one-third to one-half (for $\Omega_0 = 1$–0) of the age of the universe.

2. OBSERVATIONS

Two galaxies were observed in 1994 September as part of a program described in Forbes et al. (1996). The other seven galaxies were studied in 1995 May (see Koo et al. 1996 for details) as part of the Deep Extragalactic Evolutionary Probe project (DEEP; Mould 1993; Koo 1995). WFPC2 images are available for both programs in the F606W (V_{606}) and F814W (I_{814}) filters. Spectra were acquired with the Low Resolution Imaging Spectrograph (LRIS; Oke et al. 1995). The red-blazed 600 line mm^{-1} grating and a 2048×2048 pixel CCD with scales of 1.26 Å and 0.″215 per pixel were used. The four brightest galaxies were observed in long-slit mode with a 1.″0 slit for 30 minutes each. The other five were observed through a multiobject slitmask with a slit width of 1.″25 and exposures totaling 1–3 hours. Seeing was approximately 0.″8 and 0.″95 (FWHM) for the 1994 and 1995 observations, respectively. The spectral range varied between 4800–7400 Å for the Forbes et al. objects, 6200–8800 Å for the remaining long-slit observations, and approximately 7800 Å–1.0 μm for the slitmask data. Since the primary goal for all the spectroscopic observations was to obtain redshifts, no attempt was made to align the slits with the major axis of each galaxy. Consequently, we must consider the effects of slit misalignment during the analysis.

[1] Based on observations obtained at the W. M. Keck Observatory, which is operated jointly by the California Institute of Technology and the University of California.

[2] Based in part on observations with the NASA/ESA *Hubble Space Telescope*, obtained at the Space Telescope Science Institute, which is operated by AURA, Inc., under NASA contract NAS 5-26555.

TABLE 1

GALAXY PARAMETERS

ID Number (1)	Type (2)	z (3)	Scale (kpc arcsec^{-1}) (4)	r_d (kpc) (5)	R_f (kpc) (6)	$\Delta\theta$ (deg) (7)	Inclination (deg) (8)	$I^{\rm obs.}$ (mag) (9)	$V-I^{\rm obs.}$ (mag) (10)	A_B^a (mag) (11)	A_B^b (mag) (12)	$B-V^{\rm rest}$ (mag) (13)	$M_B^{\rm rest}$ (mag) (14)	$V_{\rm term}$ (km s^{-1}) (15)
074−2262	SBcd	0.0794	1.37	⋯	11.5	0	⋯	17.99	0.56	⋯	⋯	0.24	−19.3	⋯
074−2237	Sb	0.1535	2.41	3.2	9.7	14	80	17.93	0.77	0.96	1.45	0.36	−21.5	200^{+25}_{-15}
084−2833	Sb	0.3660	4.50	3.0	12.0	66	53	21.03	0.68	0.42	0.42	0.24	−19.8	220^{+99}_{-50}
0305−00115	Sc	0.4761	5.24	5.1	11.5	2	46	19.10	1.18	0.37	0.30	0.59	−21.7	215^{+40}_{-15}
0305−00114	D.N.	0.4762	5.24	1.8	10.0	3	56	20.20	0.94	0.45	0.48	0.38	−20.7	180^{+25}_{-30}
104−4024	Sbc	0.8116	6.74	8.1	18.5	25	85	22.17	1.66	0.96	2.01	0.67	−21.0	290^{+50}_{-40}
064−4442	Sbc	0.8770	6.94	3.2	24.9	56	60	22.07	0.99	0.49	0.57	0.24	−20.7	200^{+80}_{-40}
094−2210	Sbc	0.9000	7.01	5.7	13.3	19	60	21.41	1.34	0.49	0.57	0.44	−21.7	290^{+50}_{-25}
064−4412	Sc	0.9877	7.24	4.1	15.5	12	68	22.38	1.56	0.61	0.81	0.76	−21.4	265^{+30}_{-30}

NOTE.—Columns: (1) Galaxy identification number (Koo et al. 1996; Forbes et al. 1996); (2) Hubble type (error = 2 half-bins; D. N. = double nuclei); (3) redshift; (4) physical scale of 1″; (5) disk scale length (error = 15%); (6) radial extent of rotation curve (along major axis); (7) slit angle offset from major axis (error ∼ 10°); (8) inclination from I_{814}, cos $i = b/a$ (error ∼ 10°); (9) observed total I-band magnitude (error ∼ 0.1 mag); (10) observed $V-I$ color (error ∼ 0.15 mag); (11) internal extinction correction in the form of Tully & Fouqué 1988 (error ∼ 0.1 mag); (12) internal extinction correction in the form of Rubin et al. 1985 (error ∼ 0.1 mag); (13) rest frame $B-V$ color, A_B^a applied (error ∼ 0.2 mag); (14) absolute B magnitude corrected to zero redshift, A_B^a applied (error = 0.2 mag), note that L^* corresponds to $M_B \sim -20.4$; (15) terminal velocity ($V_{\rm term}$) from rotation curve and errors; $H_0 = 75$ km s^{-1} Mpc^{-1} and $q_0 = 0$ assumed throughout.

3. DATA REDUCTION AND ANALYSIS

3.1. *Initial Data Reduction and Sample Selection*

Pixel-to-pixel variations were removed by subtraction of a constant bias level and division with flat-fields generated from dome-flat images taken with the grating but *without* a slit. The LRIS CCD suffers from fringing at a level of up to 5% peak-to-peak in the far red, so the spectra were also divided by an appropriate fringing flat taken through the same slits and grating angles as the observations. This reduces fringing by a factor of 4, but fringing still remains a problem in the presence of strong night-sky lines. The slitmask spectra were then corrected for slit profile variations due to small irregularities along the slit edges and for instrumental distortions as determined from night-sky emission lines and the ends of slitlets. Wavelength calibrations were based on the stronger night-sky OH emission lines (Vogt 1995). The spectra were then examined for spatially extended emission lines. Seven of the 41 objects in the May 1995 redshift survey (Koo et al. 1996) had such lines, and they were augmented with the two spatially resolved sources from Forbes et al. (1996).

The *HST* images were reduced using IRAF-based reduction and analysis techniques (Forbes et al. 1994; Phillips et al. 1996). Total magnitudes and colors were measured from aperture growth curves from V_{606} and I_{814} data; inclination and position angles were estimated from the outer elliptical isophotes, and disk scale lengths were measured along the major axis as part of bulge-to-disk decompositions. Error estimates are noted in Table 1, and discussed in detail in Phillips et al. 1996.

3.2. *Measuring the Line-of-Sight Rotation Velocity*

To improve the signal-to-noise ratio (S/N), the raw rotation curves were smoothed with a 3 pixel (0.″65) boxcar along the spatial axis before measurement. At each position along the slit, we then fit Gaussian profiles to the strongest emission lines observed, ranging from Hα for the lowest-z objects through Hβ and the [O III] λ5007 line, to the [O II] λ3727 doublet for sources with $z \sim 1$. The fitting algorithm (Vogt 1995) derives the position, amplitude, width, and a linear background for a best-fit single Gaussian (double Gaussian for the [O II] doublet, with rest frame centers fixed at 3726.2 and 3728.9 Å) and calculates S/N for these parameters. Three galaxies were spatially extended in more than one emission line, and a weighted average rotation velocity was calculated. A velocity profile was calculated wherever the Gaussian fit met certain minimum requirements in profile height and width (5 σ and 3 σ); the typical value was 10 σ for both width and amplitude fits (see details in Vogt 1995). The widths were also constrained to a physically reasonable range (1–10 Å). The faint galaxy 064−4412 required a relaxation of height and width requirements to 1 σ (with typical values of 3 σ), since the [O II] line strength was quite weak.

3.3. *Estimating the True Rotation Velocity*

Determining the rotation curves of these distant galaxies poses some special difficulties not encountered with nearby galaxies. The galaxies are typically not much larger than the seeing disk (∼0.″8–1.″0) or the slit width (1.″0–1.″25), so the resultant spectra represent a complex combination of the spatial distribution in both velocity and emission line surface brightness. Moreover, the slit is usually misaligned with the major axis.

To interpret the data, we adopt a simple exponential disk model for each source, where the inclination and orientation relative to the slit matches measurements from the *HST* images. The velocities in the model are assumed to rise linearly with radius out to one disk scale length and then to remain flat (see Persic & Salucci 1991). The spatial distribution of the emission-line flux is assumed to follow the disk (Kennicutt 1989), although Ryder & Dopita (1994) find a longer scale length than that of the continuum flux. Thus, a scale length of 1.5 times that measured from the *HST* images was used. The model was then convolved with an appropriate Gaussian to approximate the seeing, masked with a model slit, and a spectral line profile calculated at each pixel along the slit. The resulting model emission line was subjected to the same analysis as the observed lines. Iterative adjustments to the circular velocity of the model were made manually until the simulated and observed emission lines matched at the velocity extremes. The model circular velocity, $V_{\rm circ}$, was then

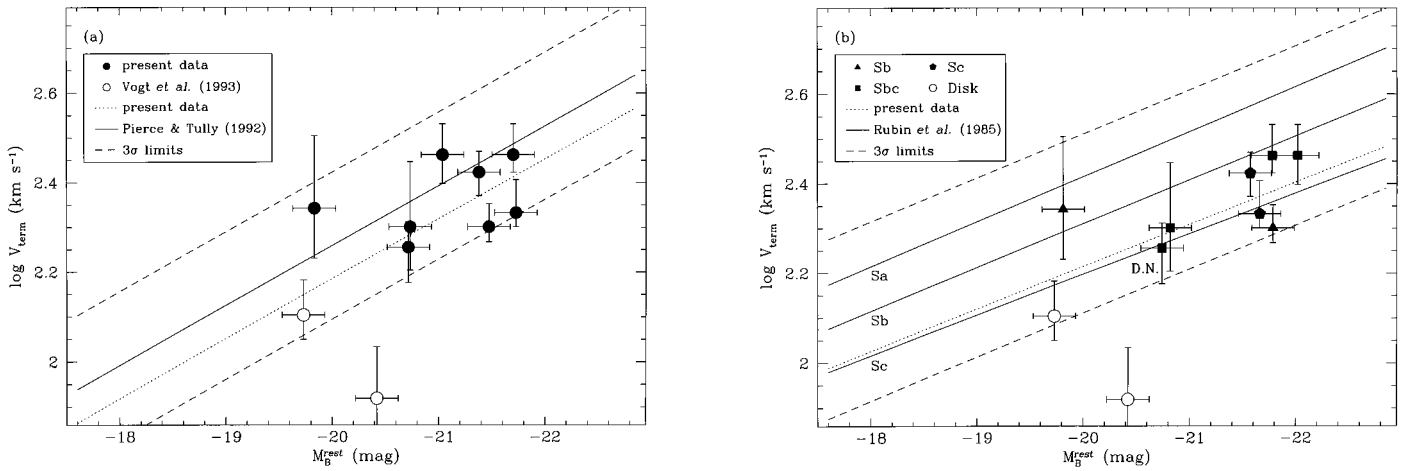

FIG. 2.—Tully-Fisher diagrams. We show our data and sources taken from Vogt et al. (1993) compared to (*a*) the Pierce & Tully (1988, 1992) relationship based on H I velocity width measurements for a restricted set of cluster spirals; and (*b*) the relationships for Sa, Sb, and Sc field galaxies found by Rubin et al. (1985) from Hα emission line studies. In (*a*) the best-fit *B*-band relation (*solid line*) and 3 σ limits (*dashed lines*) from Pierce & Tully are shown. The weighted fit to our eight Tully-Fisher candidate galaxies (*dotted line*; assuming the same slope) produces an offset of 0.55 ± 0.16 mag. In (*b*) the best-fit *B*-band relations (*solid lines*) for galaxies of type Sa, Sb, and Sc from Rubin et al. and 3 σ limits (*dashed lines*) for the complete set of nearby spirals are given. The weighted fit to our eight Tully-Fisher candidate galaxies (*dotted line*) relative to the average of the Sb and Sc relations produces an offset of 0.38 ± 0.22 mag. In each case, data have been corrected for internal extinction in a manner consistent with the local TF study; $M_B^{\rm rest}$ thus differs between (*a*) and (*b*). We assume $H_0 = 75$ km s^{-1} Mpc^{-1} and $q_0 = 0$ throughout. In summary, we see only a slight offset of $\Delta M_B \lesssim 0.6$ mag toward brighter luminosities in our data.

adopted as the intrinsic terminal velocity, $V_{\rm term}$, of the galaxy. The 1 σ errors in $V_{\rm term}$ shown in Figure 2 below were estimated by varying the inclination and position angle of each galaxy by $\pm 10°$ and adopting the extrema. Varying the distance to the elbow radius of the modeled rotation curve by 25% had a minimal effect upon the value of $V_{\rm term}$. Although the model was adjusted in amplitude to fit the velocities in the outer regions of the galaxies, in most cases it provided a good fit at all galactocentric radii.

4. RESULTS

The data for the nine sample galaxies are listed in Table 1). Coordinates can be found for all galaxies in Koo et al. (1996) and Forbes et al. (1996). We assume $H_0 = 75$ km s^{-1} Mpc^{-1} and $q_0 = 0$, though unphysical, to set upper limits on luminosity evolution. Rest-frame *BVRI* luminosities were derived from the $V_{606} - I_{814}$ color and redshift to select a model (nonevolving) spectral energy distribution from the set described in Gronwall & Koo (1995). The models are based on those of Bruzual & Charlot (1993). Galaxies were corrected for Galactic extinction, assuming extinction at I_{814} is 0.45 A_B and at V_{606} is 0.67 A_B, and for internal extinction, following the methods of Tully & Fouqué (1985) and Rubin et al. (1985), as listed in Table 1. These extinction corrections were applied consistently with the authors' prescriptions, to facilitate our final comparisons to local TF relations.

Images of the galaxies (Fig. 1 [Pl. L5 and L6]) show them to be mainly normal spirals except for 0305−00114, which has double nuclei, and a few others with asymmetries. Figure 1 also shows the observed rotation curves, the size and orientation of each slit, and the adopted model rotation curves fit to the data. The caption includes notes for individual galaxies, but 074−2262 deserves special comment. This low-luminosity galaxy resembles a highly inclined, late-type barred spiral with obvious spiral arms, bright knots of star-forming regions, and highly elongated outer isophotes, but the lack of radial velocity variations greater than ±25 km s^{-1} precludes a highly inclined disk. The object is asymmetric, shows signs of tidal disturbance, and has a possible perturbing companion 10″ away on the sky. It is also possible that this is a merger in progress between two dwarf galaxies, observed perpendicular to the path of collision. This galaxy serves to illustrate that even at low redshifts, in any randomly selected sample of galaxies there exist "disk" galaxies quite unsuitable for study via the TF relation.

5. DISCUSSION

An immediate—although not surprising—result is that the shapes of the rotation curves of these high-redshift galaxies are similar to those of local galaxies. The high-redshift rotation curves are relatively symmetric, show a "solid-body" rise in the inner regions, and turn over to a relatively constant circular velocity in the outer parts. The maximum velocities (see Table 1) are comparable to those of local spirals. Rough calculations yield masses between 1 and $5 \times 10^{11}\ M_\odot$, well within the range of masses found for nearby spiral galaxies. This result, combined with the apparent disks that are obvious in the *HST* images, shows conclusively that some *massive* disk systems were in place by $z \sim 1$.

In Figure 2 we compare the data to local TF relations in the rest-frame *B* band, which corresponds to V_{606} at $z \sim 0.4$ and to I_{814} at $z \sim 0.8$ (i.e., the *k*-corrections are small). The comparison in Figure 2*a* is to the TF relation (inverse fit, i.e., $V_{\rm term}$ as a function of M_B) for 32 spiral galaxies in the Ursa Major cluster (Pierce & Tully 1988, 1992). This relationship is based on H I velocity width measurements (corrected for turbulent broadening), but we have not converted our optical-line terminal velocities to radio widths since this correction ($\lesssim$15 km s^{-1}) is small compared to the optical error (e.g., Mathewson et al. 1992; Giovanelli et al. 1996). The two sources with redshift $z \sim 0.2$ from Vogt et al. (1993) are plotted for comparison; with only ground-based imaging available, they are less well constrained in inclination. Excluding these and the peculiar source 074−2262, we compute a weighted offset

of 0.55 ± 0.16 mag relative to the B-band TF relation of Pierce & Tully, with a dispersion of 0.71 mag. This dispersion matches the quadratic summation of errors (0.65) in the logarithmic velocity widths (0.47), the rest-frame B magnitudes (0.2), and an assumed intrinsic scatter in the TF relation (0.4) (see Willick et al. 1996, and references therein), indicating that our error estimates are consistent. An analogous calculation for the I-band relation yields an offset of 0.36 ± 0.18 mag.

Figure 2*b* shows the same galaxies and the TF relation (double regression fit) for local field galaxies of Hubble types Sa, Sb, and Sc as published in Rubin et al. (1985), corrected to $H_0 = 75$ km s^{-1} Mpc^{-1}. Since our galaxy types (see Table 1) are evenly distributed between Sb and Sc, we compare to a local relation midway between the Sb and Sc, and measure an offset of 0.38 ± 0.22 mag.

Several sample selection effects and assumptions work to make these offsets upper limits. First, at high redshift, our samples are biased toward intrinsically luminous galaxies, which will affect somewhat our results with respect to TF relations (see Teerikorpi 1984). Second, we have selected spatially extended objects, which will bias our sample toward larger galaxies. Third, we have selected objects with detectable emission lines, which will bias the sample toward galaxies with stronger than average star formation—and therefore higher luminosity. Corrections for these biases would all *reduce* the true offsets. Moreover, if we have not traced the rotation curve to sufficiently large radii, we may have underestimated the maximum velocities, and if galaxies were less dusty at earlier epochs, we may have overcorrected for extinction. These errors, if present, would also *reduce* the true offsets. Finally, adopting $q_0 = 0.5$ instead of $q_0 = 0$ would decrease the rest-frame luminosities by 0.1–0.4 mag, and again reduce the true offset.

The issue of a representative local TF sample for comparison is also critical. Key factors include the photometry passband, the observations and analysis used to determine internal velocities, the selection biases due to catalog limits, the distortions due to peculiar velocities, internal extinction corrections, and the TF fitting technique (e.g., forward, inverse, or double regression). Note, however, that our sample lies in the central region ($-19.8 < M_B < -21.7$, $180 < V_{\rm term} < 290$ km s^{-1}) of the range fit in the local samples, where the differences between various fits are minimized. We assume an error due to these effects of 0.35 mag and combine this with the measured uncertainties in our offsets ($\sim$0.2) from local TF relations to arrive at an upper limit of $\Delta M_B \lesssim 0.55 \pm 0.38$ mag.

In summary, we find an offset relative to local TF relations of $\Delta M_B \sim 0.6$ mag as a strong upper limit. We do *not* see an obvious trend with redshift or morphological type, but our sample is small. Our result is compatible with other kinematic studies of field galaxies at intermediate redshifts, such as Rix, Colless, & Guhathakurta (1996), who find a brightening of 0.44 mag for blue field galaxies at $z \sim 0.3$.

Forbes et al. (1996) concluded that galaxies near $z \sim 0.5$ show a surface brightness increase of 0.6 ± 0.1 mag, while Schade et al. (1995) find a 1.2 ± 0.25 mag increase in disky galaxies at redshifts $0.5 < z < 1.2$. Since the average bulge-to-total ratio for the Schade et al. sample is $\sim$0.1, any reductions due to a significant bulge would be small. While the samples are not directly comparable, our data suggest somewhat less brightening and exclude any total (vs. surface) brightening by more than 1.5 mag at the 99% CL. The results can be reconciled if disky galaxies of similar mass were not much brighter at $z \sim 1$ than today but had slightly smaller disk scale lengths and thus higher surface brightness.

This Letter presents first results in the investigation of kinematics via rotation curves in high-redshift galaxies. We plan future observations to increase the sample size and will constrain slits to lie within 30° of the major axes. We will use this larger, higher-quality data set to focus on a better understanding of sample selection biases, and will further explore a more analogous local TF relation. Nevertheless, the current data clearly indicate that optical rotation curves can be measured up to $z \sim 1$ and will provide an important constraint on our understanding of the evolution of disk galaxies.

We thank K. Wu, R. Guzmán, and D. Kelson for aid with the spectra, and C. Mihos and J. Van Gorkom for discussions of galaxy 074−2262. DEEP was established through the Center for Particle Astrophysics. Funding was provided by NSF grants AST-922540, AST-9120005, and AST-8858203; NASA grants AR-5801.01-94A, GO-2684.04-87A, and GO-2684.05-87A. C. G. acknowledges funding from an NSF Graduate Fellowship.

REFERENCES

Aaronson, M., Bothun, G., Mould, J. R., Huchra, J., Schommer, R. A., & Cornell, M. E. 1986, ApJ, 302, 536
Broadhurst, T. J., Ellis, R. S., & Shanks, T. 1988, MNRAS, 235, 827
Bruzual, A., G., & Charlot, S. 1993, ApJ, 405, 538
Colless, M., Ellis, R. J., Taylor, K., & Hook, R. N. 1990, MNRAS, 244, 408
Colless, M. M., Schade, D., Broadhurst, T. J., & Ellis, R. S. 1994, MNRAS, 267, 1108
Forbes, D. A., Elson, R. A. W., Phillips, A. C., Illingworth, G. D., & Koo, D. C. 1994, ApJ, 437, L17
Forbes, D. A., Phillips, A. C., Koo, D. C., & Illingworth, G. D. 1996, ApJ, 462, 89
Giovanelli, R. G., et al. 1996, in preparation
Glazebrook, K. Ellis, R., Santiago, B., & Griffiths, R. 1995, MNRAS, 275, L19
Gronwall, C., & Koo, D. C. 1995, ApJ, 440, L1
Haynes, M. P., & Giovanelli, R. 1991, ApJS, 77, 331
Kennicutt, R. C. 1989, ApJ, 344, 685
Koo, D. C. 1995, in Wide Field Spectroscopy and the Distant Universe, ed. S. Maddox & A. Aragón-Salamanca (Singapore: World Scientific), 55
Koo, D. C., et al. 1996, ApJ, in press
Kron, R. 1986, in Nearly Normal Galaxies, ed. S. M. Faber (Berlin: Springer), 300
Mathewson, D. S., Ford, V. L., & Buchhorn, M. 1992, ApJS, 81, 413
Mihos, J. C. 1995, ApJ, 438, L75
Mould, J. 1993, in ASP Conf. Ser. 43, Sky Surveys: Protostars to Protogalaxies, ed. B. T. Soifer (San Francisco: ASP), 281
Oke, J. B., et al. 1995, PASP, 107, 375
Persic, M., & Salucci, P. 1991 ApJ, 368, 60
Phillips, A. C., et al. 1996, in preparation
Pierce, M. J., & Tully, R. B. 1988, ApJ, 330, 579
———. 1992, ApJ, 387, 47
Rix, H.-W., Colless, M., & Guhathakurta, P. 1996, in IAU Symp. 171, New Light on Galaxy Evolution, ed. R. Bender & R. L. Davies (Dordrecht: Kluwer), in press
Roberts, W. W., Roberts, M. S., & Shu, F. H. 1975, ApJ, 196, 381
Rubin, V. C., Burstein, D., Ford, W. K., & Thonnard, N. 1985, ApJ, 289, 81
Ryder, S. D., & Dopita, M. A. 1994, ApJ, 430, 142
Schade, D., Lilly, S. J., Crampton, D., Hammer, F., Le Fèvre, O., & Tresse, L. 1995, ApJ, 451, L1
Teerikorpi, P. 1984, A&A, 141, 407
Tully, R. B., & Fisher, J. R. 1977, A&A, 54, 661
Tully, R. B., & Fouqué, P. 1985, ApJS, 58, 67
van der Kruit, P. C., & Pickles, A. J. 1988, in Towards Understanding Galaxies at High Redshift, ed. R. G. Kron & A. Renzini (Hingham: Kluwer), 339
Vogt, N. P. 1995, Ph. D. thesis, Cornell University
Vogt, N. P., Herter, T., Haynes, M. P., & Courteau, S. 1993, ApJ, 415, L95
Willick, J. A., Courteau, S., Faber, S. M., Burstein, D., Dekel, A., & Kolatt, T. 1996, ApJ, 457, 460

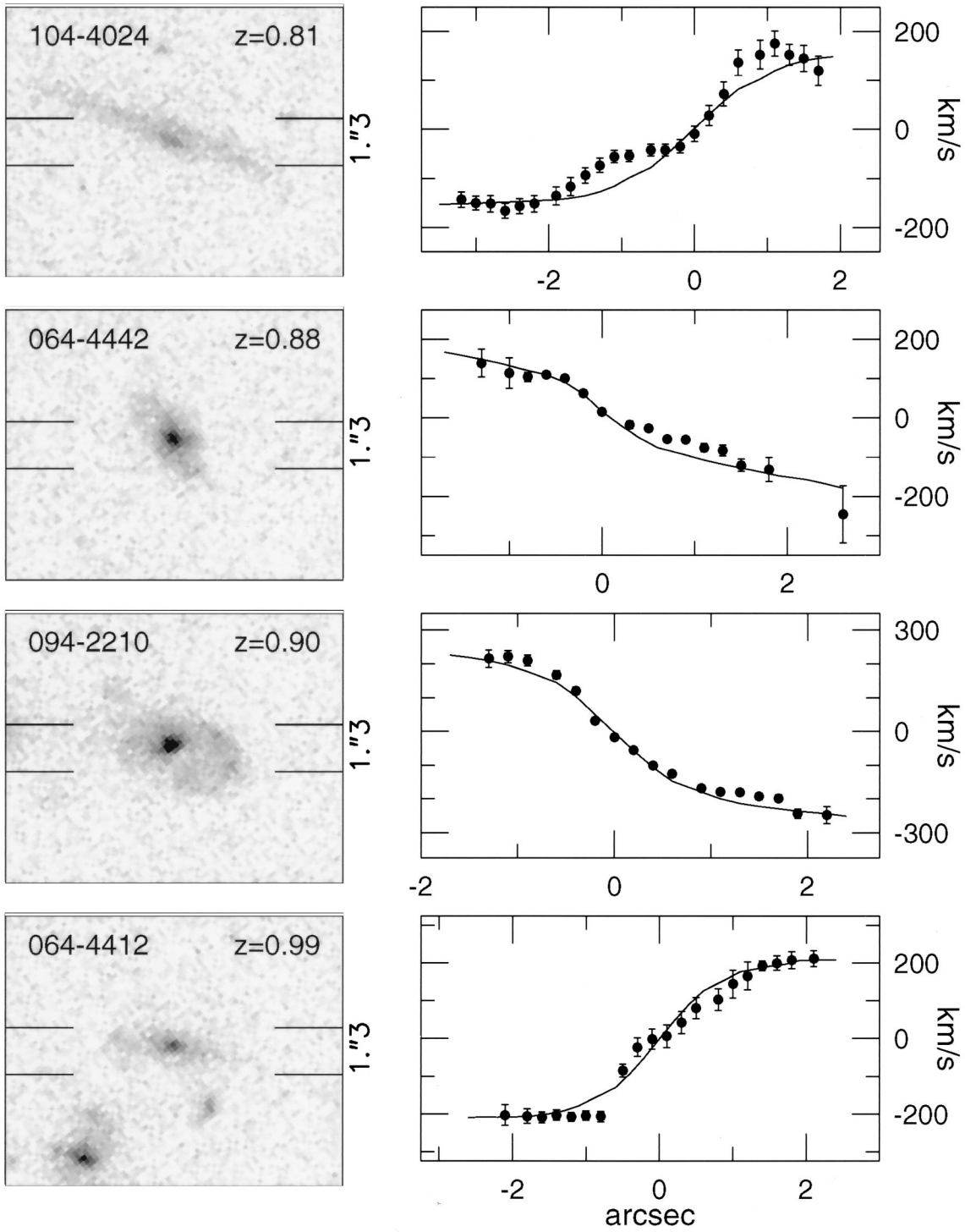

FIG. 1.—I_{814}-band images and observed velocity curves for the nine sample galaxies. For each galaxy, the LRIS slit width and orientation are indicated on the WFPC2 image on the left. In the velocity information on the right, points represent the observed velocities and the solid line is the model rotation curve. Error bars are internal errors derived from the line-fitting technique. The velocity curves are measured from Hα for sources with redshift $z < 0.4$ and from [O II] λ3727 for $z > 0.4$ (*filled circles*). We also present [O III] λ5007 for galaxy 084−2833 and Hβ for sources 0305−00115 and 0305−00114 (*open circles*). Some individual notes: (074−2262) see text; (074−2237) we suffer significant slit losses from slit misalignment (14°) due to large spatial extent, and see an *apparent* slope in the outer regions of the observed spectrum though terminal velocity is achieved well within the velocity profile; (084−2833) Hα and [O III] flux distribution and velocities match well in spatial extent, though the large position angle correction makes the estimate of the terminal velocity uncertain; (0305−00115) [O II] data (*open circles*) are of poorer quality than the Hβ data (*filled circles*), and should be discounted; (0305−00114) double nucleus and strong emission line spectra suggests a merger in progress, though there is no apparent distortion in the velocity profile and the faint outer isophotes are undisturbed (though lack of faint tidal features may be a surface brightness dimming effect, (see Mihos 1995); (104−4024) evident dust lane, and low (S/N) [O II] doublet; (094−2210) luminous ($M_B = -21.7$) galaxy with a clear disk, high (S/N) [O II] doublet.

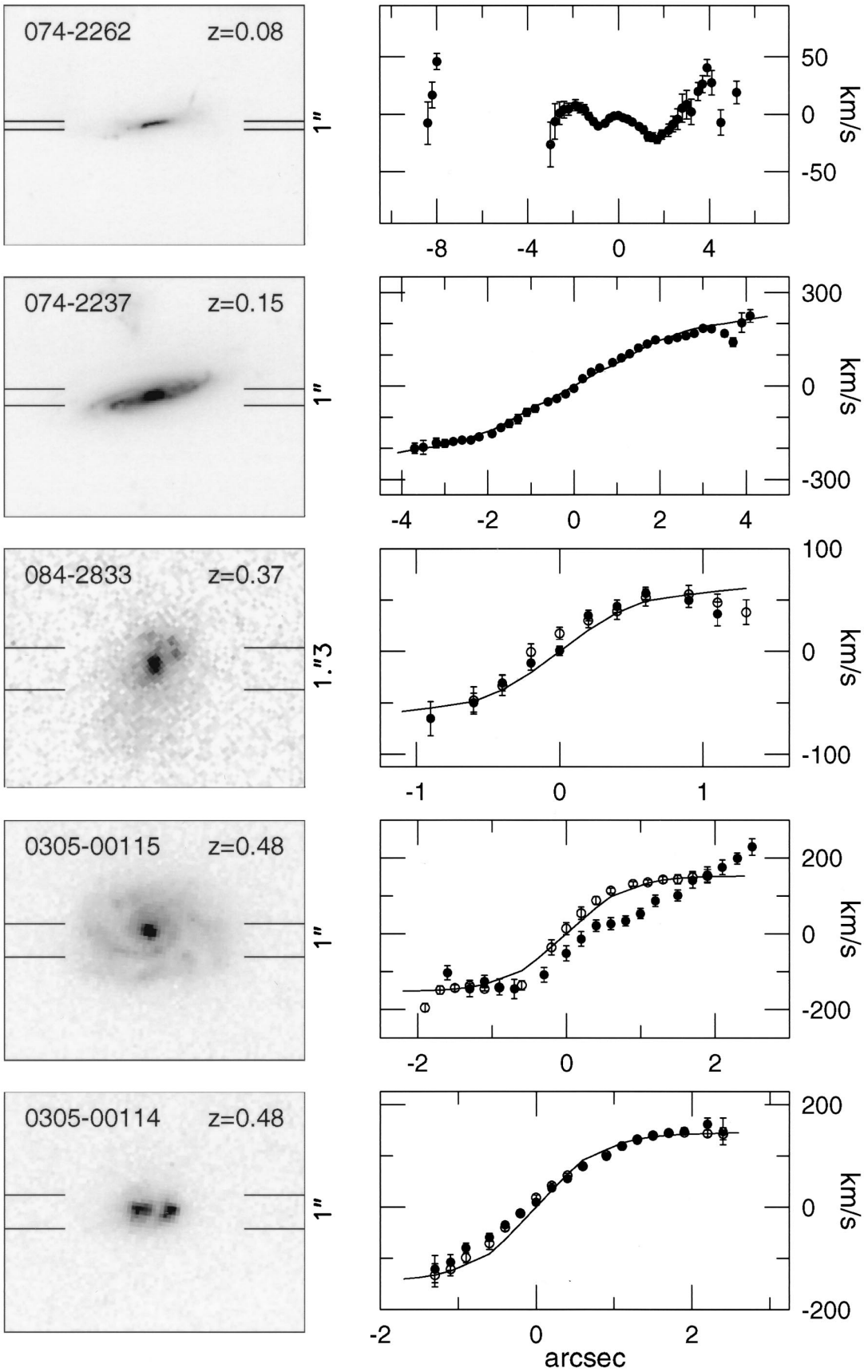

FIGURE 1— Continued